World Academy of Science, Engineering and Technology
International Journal of Mathematical and Computational Sciences
Vol:1, No:9, 2007

Global Behavior in $(Q - xy)^2$ Potential

K. Jaroensutasinee

***Abstract*— The general global behavior of particles in a nonlinear $(Q - xy)^2$ potential cannot be revealed by a Poincaré surface of section method (PSS) because most trajectories take practically infinitely long time to integrate numerically before they come back to the surface. In this study, as an alternative to PSS, a multiple scale perturbation is applied to analyze global adiabatic, non-adiabatic and chaotic behavior of particles in this potential. It was found that the results can be summarized as a form of a Fermi-like map. Additionally, this method gives a variation of global stochasticity criteria with Q.**

***Index Terms*— Multiple Scale Perturbation, The Poincaré Surface of Section, Fermi Map**

I. Introduction

NORMALLY the Poincaré surface of the section method (PSS) can be applied in order to reduce the dimension of the phase space of a 2D nonlinear Hamiltonian system to make it possible to obtain a qualitative description as provided by a phase plane analysis. However, for a simple nonlinear dynamical system where the effective Hamiltonian potential is $V(x, y) = (Q - xy)^2$, the PSS method can be impractical to provide such descriptions. This is because for this kind of system most trajectories can execute infinitely long times before they cut the required section again. The purpose of this study is to analyze such a case and to propose a combination of analytical and computational methods to obtain a global description of the system.

This form of potential when $Q = 0$ is studied as a starting point to understand the convergence to a billiard [1]. In addition, it had been long thought that this form of potential had an ergodic property until a series of small stable islands in this system were found [2], [3]. This is illustrated in Fig. 1. For the case $Q = 0$, it is possible to approximate the trajectory away from the center in the form of Bessel functions and trajectories on either side of the center can be connected by a simple line approximation. From these orbits a map can be derived which has chaotic solutions [4]. This signifies that a major portion in phase space close to these Bessel trajectories is chaotic.

It is important to note that this form of potential has another origin namely from the field of plasma confinement. The same potential can be derived from the motion of a charged particle in a cusp magnetic field [5], [6]. Using this picture of a charge particle in a magnetic field gives us more information and more insight into this nonlinear potential.

Manuscript received November 30, 2006; revised November 30, 2006. This work was partly supported by the Thailand Research Fund, through the Post-Doctoral Grant (PDF/62/2540).

K. Jaroensutasinee is with Complex System Research Unit, Institute of Science, Walailak University, Nakhon Si Thammarat 80161, Thailand (e-mail: krisanadej@gmail.com, web site: http://computing.wu.ac.th).

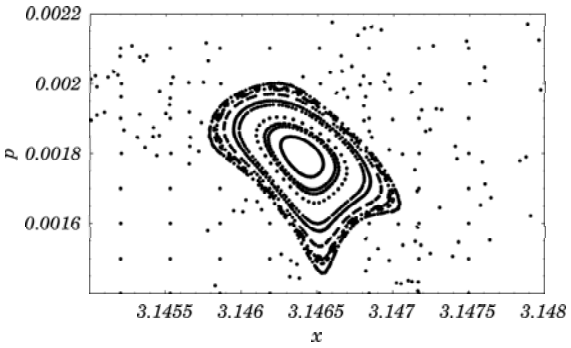

Fig. 1. Poincaré Surface of Section for $Q = 0$. The stable islands occupies very small area of the phase space while most areas of PSS are chaotic.

In general, the behavior of charged particle motion in a magnetic bottle can be thought of as being composed of two oscillations, the longitudinal oscillation along the guiding center and the cyclotron motion. Unfortunately, the complete analytical solution of such situation is extremely difficult or impossible to obtain. One, therefore, has to search for approximate solutions. In this work multiple-time perturbation theory is used to study the adiabatic, non-adiabatic and chaotic behavior of charged particles in a linear cusp magnetic field where the effective Hamiltonian potential is $(Q - xy)^2$.

With a straightforward perturbation scheme, one finds that some terms in the expansion are not periodic in time and in fact blow up as t gets large (secular behavior). These troublesome terms can usually be algebraically combined to restore periodicity and this is the basis of the multiple time analysis. The method adopted here is based on the observation that the two frequencies referred to above are quite distinct. Hence in this situation a multiple time perturbation scheme is ideally suited. The underlying idea of the multiple time perturbation is to extend the time variable to two or more independent variables representing different timescales. The expansion is then carried out in the usual way and the additional freedom of having two timescales is used to remove any time secularities.

II. Adiabatic and Non-adiabatic Trajectories

When this potential is thought of in terms of a charged particle moving in a cusp magnetic field, it is important to realize that the particle is confined to zones depending on its initial spatial and momentum conditions. In fact, these confinement zones become like magnetic bottles. The fast oscillation is associated with the Larmor frequency whilst the slow oscillation is associated with the sloshing in the magnetic bottle. Fig. 2 is obtained from a typical numerical solution

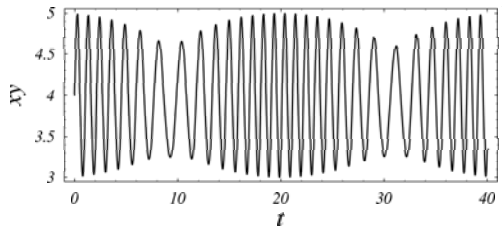

Fig. 2. Typical motion of a particle for $Q = 4$.

for $Q = 4$ and shows two distinctive oscillations with two distinctive timescales.

With this idea in mind, the hyperbolic co-ordinate system is the most appropriate as one of the co-ordinates essentially describes the guiding center motion. It was first used by [7] to calculate the non-adaibatic jumps.

The transformation equations between the hyperbolic and the Cartesian co-ordinate system are:

$$\begin{array}{llll} \psi & = xy, & \phi & = \frac{1}{2}\left(x^2 - y^2\right), \\ \Psi & = \frac{d\psi}{dt} = qx + py, & \Phi & = \frac{d\phi}{dt} = px - qy, \end{array} \tag{1}$$

or

$$\begin{array}{ll} x & = \pm\sqrt{\phi + \sqrt{\phi^2 + \psi^2}}, \\ y & = \pm\sqrt{-\phi + \sqrt{\phi^2 + \psi^2}}, \\ p & = \frac{dx}{dt} = \pm\frac{\Phi\psi + \Psi(-\phi + \sqrt{\phi^2+\psi^2})}{2\sqrt{\phi^2+\psi^2}\sqrt{-\phi+\sqrt{\phi^2+\psi^2}}}, \\ q & -\frac{dy}{dt} - \pm\frac{(\Phi\psi + \Psi(\phi + \sqrt{\phi^2+\psi^2})\sqrt{-\phi+\sqrt{\phi^2+\psi^2}}}{2\psi\sqrt{\phi^2+\psi^2}} \end{array} \tag{2}$$

The equations of motion in the rectangular co-ordinate and hyperbolic co-ordinate systems are

$$\begin{array}{ll} \frac{d^2x}{d^2t} & = y(Q - xy), \\ \frac{d^2y}{d^2t} & = x(Q - xy), \\ \frac{d^2\psi}{d^2t} & = 2\sqrt{\phi^2 + \psi^2}(Q - \psi) + \frac{\psi(\Psi^2 - \Phi^2) + 2\phi\Phi\Psi}{2(\phi^2+\psi^2)}, \\ \frac{d^2\phi}{d^2t} & = \frac{\phi(\Phi^2 - \Psi^2) + 2\Phi\psi\Psi}{2(\phi^2+\psi^2)} \end{array} \tag{3}$$

Next the Hamiltonian can be used to determine the total energy of the particle. In the rectangular co-ordinate system,

$$H = \tfrac{1}{2}((\tfrac{dx}{dt})^2 + (\tfrac{dy}{dt})^2 + (Q - xy)^2) \tag{4}$$

and in the hyperbolic co-ordinate system,

$$H = \tfrac{1}{2}(\tfrac{\Phi^2+\Psi^2}{2\sqrt{\phi^2+\psi^2}} + (Q - \psi)^2) = E \tag{5}$$

in which the total energy E can be normalized to $1/2$ without loss of generality.

The magnetic moment, defined by $\mu = v_\perp^2/B$ where $v_\perp$ is the component of the velocity perpendicular to the direction of the local magnetic field, can be written in rectangular co-ordinates as

$$\mu = \frac{(qx+py)^2}{(x^2+y^2)^{\frac{3}{2}}} + \frac{(Q-xy)^2}{\sqrt{x^2+y^2}} \tag{6}$$

and in hyperbolic co-ordinates as

$$\mu = \frac{\Psi^2}{2^{\frac{3}{2}}(\phi^2+\psi^2)^{\frac{3}{4}}} + \frac{(Q-\psi)^2}{\sqrt{2}(\phi^2+\psi^2)^{\frac{1}{4}}} \tag{7}$$

Also it is worth considering the time derivative of the magnetic moment $d\mu/dt$. It is found that in the hyperbolic system

$$\begin{array}{ll} \frac{d\mu}{dt} & = \frac{1}{2^{7/2}(\phi^2+\psi^2)^{7/4}}\left[2\phi\Phi\Psi^2 - 2\psi\Psi^3 - 4\psi\Phi^2\Psi\right. \\ & \left. -4(\phi^2+\psi^2)(\phi\Phi + \psi\Psi)(Q-\psi)^2\right] \end{array} \tag{8}$$

The perturbation scheme starts by introducing two timescales [8],

$$\tau_i = \epsilon^i\tau, \tag{9}$$

where $i = 0$ and 1 after the following transformation is introduced:

$$\begin{array}{ll} t \to \tau: & t = \frac{1}{\sqrt{Q}}\tau, \frac{d\tau}{dt} = \sqrt{Q}, \\ \psi \to m: & \psi = Qm, \frac{d\psi}{dt} = Q\sqrt{Q}\dot{m} \\ \phi \to s: & \phi = Qs, \frac{d\phi}{dt} = Q\sqrt{Q}\dot{s}. \end{array} \tag{10}$$

Total derivatives with respect to τ can now be expanded in terms of partial derivatives with respect to the τ_i,

$$\begin{array}{lll} \frac{d}{d\tau} & = & \frac{\partial}{\partial\tau_0} + \epsilon\frac{\partial}{\partial\tau_1} = \partial_0 + \epsilon\partial_1, \\ \frac{d^2}{d\tau^2} & = & \frac{\partial^2}{\partial\tau_0^2} + 2\epsilon\frac{\partial^2}{\partial\tau_0\partial\tau_1} + \epsilon^2\frac{\partial^2}{\partial\tau_1^2} \\ & = & \partial_{00}^2 + 2\epsilon\partial_{01}^2 + \epsilon^2\partial_{11}^2, \end{array} \tag{11}$$

in which the notation ∂_{ij} is introduced.

Both s and m are expanded in powers of ϵ and

$$\begin{array}{lll} s & = & s_0(\tau_1) + \epsilon s_1(\tau_0,\tau_1) + \epsilon^2 s_2(\tau_0,\tau_1) + ..., \\ \psi & = & m_0(\tau_1) + \epsilon m_1(\tau_0,\tau_1) + \epsilon^2 m_2(\tau_0,\tau_1) + ... \end{array} \tag{12}$$

where the small parameter (ϵ) used in the perturbation scheme is defined as $1/Q$.

By inserting the above expansion scheme into the basic equations (3) and equating terms of the same order in ϵ gives equations for $s_0, s_1, ...$ and $m_0, m_1, ...$ To zero order m_0 is constant and equal to 1.

To first order the following important differential equation was derived:

$$\partial_{00}^2 m_1 = -2\sqrt{s_0^2 + 1}\, m_1, \tag{13}$$

whilst to second order

$$\begin{array}{l} 2(s_0^2+1)(\partial_{00}^2 s_2) = \\ \quad -s_0 A_1^2\omega_0^2\cos(2\omega_0\tau_0 + 2C_{m_1}) \\ \quad +2\partial_1 s_0 A_1\omega_0\cos(\omega_0\tau_0 + C_{m_1}) \end{array} \tag{14}$$

with the consistency condition

$$(s_0^2+1)\partial_{11}^2 s_0 = \frac{3}{4}s_0(\partial_1 s_0)^2 - \frac{1}{2}s_0\sqrt{1+s_0^2}, \tag{15}$$

which removes secular behavior. The solution to (13) namely $m_1 = A_1(\tau_1)\sin(\omega_0\tau_0 + C_{m_1}(\tau_1))$ where $\omega_0^2 = 2\sqrt{s_0{}^2+1}$ has been used to obtain (14). A_1 and C_{m_1} are possibly functions of τ_1 but are constant with respect to τ_0. It is possible to determine A_1 from the energy equation by substituting the above forms for s_0, m_1 and s_2 into the energy equation. It was found that

$$A_1^2 = 1 - \frac{(\partial_1 s_0)^2}{2\sqrt{1+s_0^2}}. \tag{16}$$

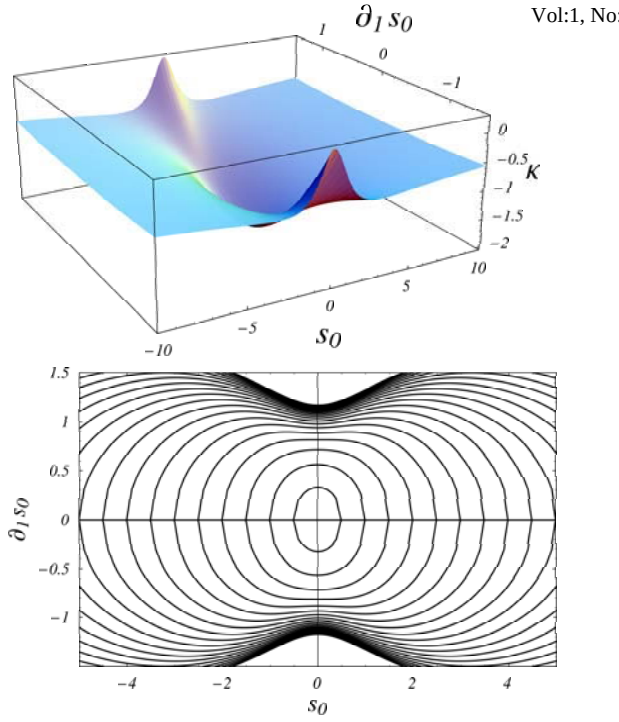

Fig. 3. 3D surface of κ (top) and phase space for s_0 (bottom). Each contour represents a different value of κ, and hence μ.

A. Phase Space for Large Timescale Motion

Considering (15), although it seems impossible to solve the differential equation in closed forms, it is possible to obtain an analytic description of the phase space for s_0. The equation may be integrated once and reduced to

$$(\partial_1 s_0)^2 = \kappa(1+s_0^2)^{3/4} + 2\sqrt{1+s_0^2}, \tag{17}$$

where κ is a constant that is determined by initial conditions.

With the condition that $s_0 = s_{0,m}$ when $\partial_1 s_0 = 0$,

$$\kappa = -2(s_{0,m}^2+1)^{-1/4} \tag{18}$$

or

$$s_{0,m} = \pm\sqrt{(-\frac{2}{\kappa})^4 - 1}. \tag{19}$$

These imply that the value of $\partial_1 s_0$ when $s_0 = 0$ is given by

$$\partial_1 s_0 \mid_{s_0=0} = \pm\sqrt{2+\kappa}. \tag{20}$$

and $\partial_1 s_0 \mid_{s_0=0}$ was related to $s_{0,m}$ by eliminating κ to give

$$(\partial_1 s_0 \mid_{s_0=0})^2 = -2(1+s_{0,m}^2)^{-1/4} + 2. \tag{21}$$

This equation can be interpreted physically as it determines the maximum distance that the particle can reach away from the median plane ($x = y, s_0 = 0$) with a given velocity $\partial_1 s_0 \mid_{s_0=0}$ at the median plane ($s_0 = 0$). In the limit as $s_{0,m} \to \infty$, $(\partial_1 s_0 \mid_{s_0=0})^2 \to 2$. This means that the particle position can tend to infinity if the injected velocity at the median plane approaches 2.

It was also possible to relate κ to the magnetic moment. To the lowest order ($\epsilon^{\frac{1}{2}}$), the magnetic moment is

$$\mu = \epsilon^{1/2}\left[\frac{(\partial_0 m_1)^2}{2^{3/2}(1+s_0^2)^{3/4}} + \frac{m_1^2}{\sqrt{2}(1+s_0^2)^{1/4}}\right]. \tag{22}$$

Substituting in our expansions for s_0 and m_1 yields

$$\mu = -\epsilon^{1/2}\frac{\kappa}{2^{3/2}} \tag{23}$$

and so μ is a constant to this order (the lowest order) and the motion is adiabatic.

The phase plane can be mapped using (17) and is shown in Fig. 3. This phase plane is generated with a constant step size in κ. The noticable two dark bands appearing near the top and bottom of the center exhibit a so-called "squeezing effect". A particle trajectory will lie on one of the outer contours if it is injected from a great distance and corresponds to a small value of κ and hence of the magnetic moment. When such a particle reaches the median plane where $s_0 = 0$, a tiny variation due to higher order terms in the expansion can take the particle to another contour with a different value of the magnetic moment since the contours are all close to each other due to the squeezing effect. This provides the opportunity for non-adiabatic and chaotic effects to take place. In short the presence of the squeezing of orbits is the indication that chaotic effects are to be found. This squeezing effect is in fact related to the overlapping resonance effect in the standard map. This will be illustrated later in this study when a Fermi-like map from this representation was derived.

B. Comparison of the method with numerically integrated orbits (for $Q > 1$)

From the perturbation analysis, to second order

$$\begin{aligned} t &= \sqrt{Q}\tau_1 = \tfrac{1}{\sqrt{Q}}\tau_0 \\ \psi &= Qm = Q + m_1 \\ \phi &= Qs = Qs_0 + \tfrac{1}{Q}s_2 \end{aligned} \tag{24}$$

which can be used to specify the initial conditions in the numerical comparison with the full orbits.

To avoid the squeezing effect around the median plane, it is more appropriate to start the particle far away from the plane. This can be achieved by setting $s_0(0) = s_{0,m}$, with the initial velocity $\partial_1 s_0(0) = 0$. Moreover, the initial conditions take the form $s_0 = s_{0,m}, s_1(0) = s_2(0) = \partial_1 s_0(0) = 0$, and $\partial_0 m_1(0) = (2\sqrt{s_{0,m}^2+1})^{1/2}$ and in the original set of variables $\phi(0) = Qs_{0,m}, \psi(0) = Q, \Phi(0) = 0$ and $\Psi(0) = (2Q\sqrt{\phi_{0,m}^2+1})^{1/2}$. With these initial conditions (15) and the energy equation, then the system is ready to be integrated numerically.

The verification was began with $Q = 10$ and found that the slow time-scale oscillation was perfectly described by the numerical solution of ϕ_0. The amplitude of the oscillation in ψ is also fully governed by A_1 which is a function of the slow timescale.

For the fast time-scale, there is still some disagreement. This is due to phase shifts in the fast time-scale. Better agreement can be obtained by redefining the phase in m_1 by writing

$$m_1 = A_1(\tau_1)\sin\left(\frac{1}{\epsilon}\int_0^{\tau_0}\omega_0(\tau)d\tau\right) + C_1. \tag{25}$$

This is consistent with the multiple time expansion.

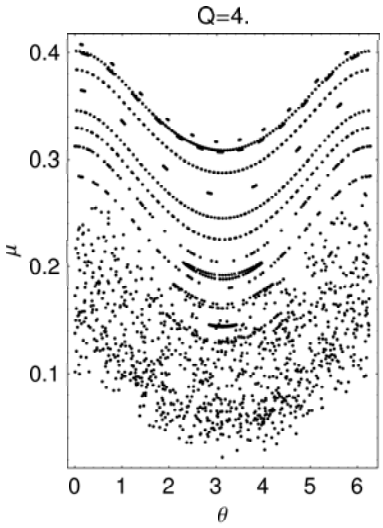

Fig. 4. Poincaré Map on x=y plane for $Q = 4$.

C. Non-adiabatic Behavior and Fermi-like Map

For the adiabatic limit, when the magnetic moment is nearly constant or constant to lowest order, the agreement between solutions to lowest order of the multi-time perturbation expansion and the numerical solutions of equations of motion is very good. This reflects the adiabatic behavior of the particle. However, if the particle is followed until it crosses the median plane ($\phi = 0$), such a good agreement would not be archieved and the magnetic moment of the particle changes to another value. The difference of the two values, known as the non-adiabatic jump, is not described in the adiabatic theory or the multiple-time perturbation analysis where the magnetic moment or κ should be held constant.

In Fig. 6 these sudden changes in μ as the particle crosses the $\phi = 0$ plane are shown for $Q = 4$. Away from the $\phi = 0$ plane it is seen that μ is a good constant. The small ripples could be accounted for by going to next order in the multiple time expansion.

For an orbit that starts with $d\phi/dt = 0$ (a reflection point) and μ_1 at $t = t_1$ and reaches the subsequent reflection point at t_2 with the new magnetic moment μ_2, the non-adiabatic jump in the magnetic moment $\triangle\mu = \mu_2 - \mu_1$ can be defined by integrating

$$\triangle\mu = \int_{t1}^{t2} dt \frac{d\mu}{dt}. \tag{26}$$

It was found that the $\cos\theta$ term in $d\mu/dt$ equation gives the most significant contribution to the non-adiabatic jump. For now it is desirable to neglect the other contribution. Using the definitions $v^2 = v_\perp^2 + v_\parallel^2 = 1$,

$$\begin{array}{ll} v_\parallel^2 = \frac{\Phi^2}{2\sqrt{\phi^2+\psi^2}}, & v_\perp^2 = \frac{\Psi^2}{2\sqrt{\phi^2+\psi^2}} + (Q-\psi)^2, \\ B = \sqrt{2}(\phi^2+\psi^2)^{1/4}, & \frac{1}{R_c} = \frac{\partial B}{\partial \psi}, \end{array} \tag{27}$$

and to lowest order when μ could be treated as a constant with

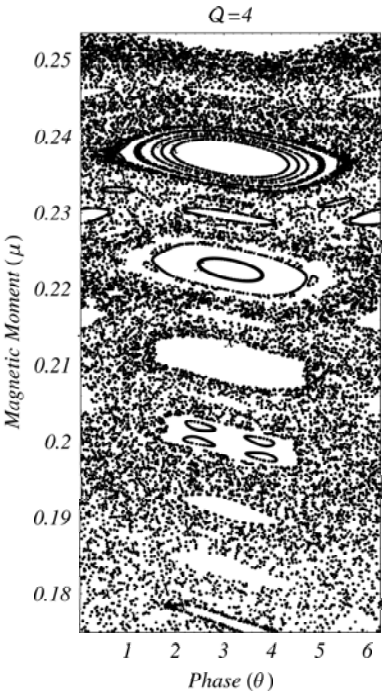

Fig. 5. Typical Fermi-like Map for $Q = 4$.

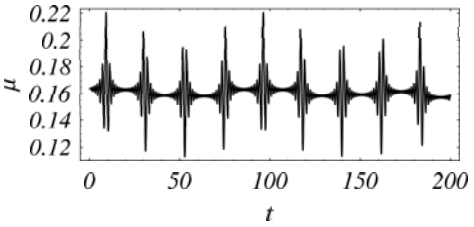

Fig. 6. Typical non-adiabatic behavior for $Q = 4$.

$v^2 = 1$,

$$\begin{array}{lcl} v_\parallel^2 & = & \frac{\partial_1 \phi_0^2}{2\sqrt{Q^2+\phi_0^2}}, \\ v_\perp^2 & = & \frac{\partial_0 \psi_1^2}{2\sqrt{Q^2+\phi_0^2}} + \psi_1^2, \\ B & = & \sqrt{2Q}(Q^2+\phi_0^2)^{1/4} = \epsilon^{-1/2}\omega_0, \\ \frac{1}{R_c} & = & \frac{2\epsilon^{1/2}}{\omega_0^3}, \end{array} \tag{28}$$

where B is the magnetic field strength and R_c is the radius of curvature of the field line. Also,

$$\frac{d\mu}{dt} = -\frac{\mu^{1/2}}{R_c B^{1/2}}(2v^2 - B\mu)\cos\theta \tag{29}$$

with the phase $\theta - \theta_0 - \epsilon^{-1}\int dt\omega_0 = \theta_0 - \int d\phi(1/v_\parallel)$. A term proportional to $\cos 2\theta$ has been neglected which can be shown to lead to second order corrections. This equation is similar to those discussed in [7] and in [9].

The integral defined by (26) can be evaluated by a contour integral method. When the domain of the integration was changed from t to ϕ using the relation $d\phi/dt = v_\parallel B$, the integral becomes a contour integral from ϕ_1 to ϕ_2. When the domain is extended to the complex plane, the contour integral

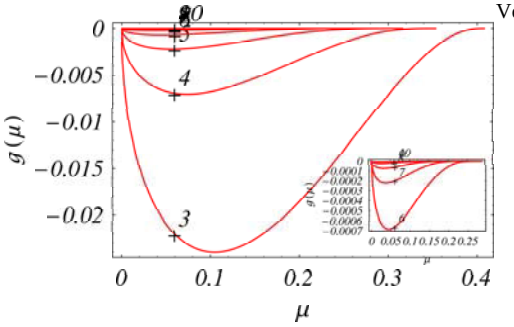

Fig. 7. Variation of $g(\mu)$ with Q (marked with + signs).

is dominated by a singularity pole with the minimum of the magnetic field strength. The integration can then be evaluated by using a general technique of contour integration in the complex plane. For this particular system, the jump can be approximated by

$$\begin{aligned}\triangle\mu &= -\frac{\pi\mu^{1/2}\epsilon^{1/8}}{\Gamma(9/8)2^{3/8}}\times \\ &\exp(-\frac{1}{\epsilon}\int_0^{\pi/2} d\theta\frac{\cos\theta}{\sqrt{1-\sqrt{\frac{2}{\epsilon}}\mu\cos^{1/2}\theta}})\cos\theta_0,\end{aligned} \tag{30}$$

where θ_0 is the phase when the trajectory crosses the median plane [7]. The terms that was neglected in above treatment is proportional to $\cos 2\theta_0$ but with a modular value of the order of the square of $\Delta\mu$.

To study the dynamics of a particle undergoing many reflections in the mirror field by solving the equations of motion is not practical in most cases. Numerical studies suggest that orbits with low values of the magnetic moment are highly chaotic, giving rise to exponential divergence (positive Lyapunov number) of the numerical solutions to the actual orbits. The alternative way to study the reflections is by using a mapping.

(30) provides us with the change in the magnetic moment for each crossing. Defining

$$\begin{aligned}g(\mu) &= -\frac{\pi\mu^{1/2}\epsilon^{1/8}}{\Gamma(9/8)2^{3/8}}\times \\ &\exp(-\frac{1}{\epsilon}\int_0^{\pi/2} d\theta\frac{\cos\theta}{\sqrt{1-a\cos^{1/2}\theta}}),\end{aligned} \tag{31}$$

with $a=\mu\sqrt{2/\epsilon}$. Then, (30) can be rewritten as

$$\triangle\mu = g(\mu_n)\cos\theta. \tag{32}$$

In order to get the complete description, the net phase change in $\theta, d(\mu)$, of the orbit executing μ was calculated. Using the result from the multi-time perturbation,

$$\begin{aligned}\triangle\theta &= d(\mu) \\ &= \frac{2}{\epsilon}\int_0^{\bar{\theta}}\frac{\cosh\theta d\theta}{\sqrt{1-a\cosh^{1/2}\theta}}\end{aligned} \tag{33}$$

where $\cosh\bar{\theta}=1/a^2$ and $s_0=\sinh\theta$.

Hence the complete description including the adiabatic and the non-adiabatic behavior is a mapping of the form, where a change of phase has been made in (32),

$$\begin{aligned}\mu_{n+1} &= \mu_n + g(\mu_n)\sin\theta_n \\ \theta_{n+1} &= \theta_n + d(\mu_{n+1}).\end{aligned} \tag{34}$$

Many applications [9], [10], [11] also give rise to a mapping of this form. Unfortunately, these mapping equations are still complex, and to gain an understanding of the general features of the map, linearization around a special value of $\bar{\mu}$ defined by the resonance condition $d(\bar{\mu})=2m\pi$ is possible where m is a positive constant. The linearization produces the Chirikov or standard map

$$\begin{aligned}I_{n+1} &= I_n + K\sin\theta_n \\ \theta_{n+1} &= \theta_n + I_{n+1}\end{aligned} \tag{35}$$

where $K = d'(\bar{\mu})g(\bar{\mu})$, $I_n = d'(\bar{\mu})\delta\mu_n$ and $'$ denotes differentiation. It is possible to give the positions of the major resonances with the corresponding $\bar{\mu}$ and distances between the resonances, and this is illustrated in Fig. 8.

However, this is not area preserving, that is, not a true representation of a Hamiltonian system. Since the above treatment is essentially an expansion in g and consistent with this expansion. The map can be made area preserving by taking

$$\theta_{n+1} = \theta_n + d(\mu_{n+1}) - g'(\mu_n\cos\theta_n). \tag{36}$$

The result of the numerical evaluation of the map given by (34) is shown in Fig. 5. It is similar to the phase plane structure of the Fermi mapping as discussed in [11]. The islands show quasi-periodic behavior of the particle around $d(\mu_m)=m\pi$ resonances when m is an even number starting from 8. If m is an odd number, a period-two resonance was obtained. They are situated between the even-number resonances. A number of bounded areas of stochasticity also exist between each resonance. However, when m is higher than 18 or μ is approximately equal to 0.22, the stochastic regions of each resonance join together, creating a global stochastic region. The charged particle can then wander to very low values of μ if it is initiated in this stochastic region.

The phase plane structure around each of the resonances is of the well known form found of the Chirikov map [11], suitably normalized, as expected from the derivation which led to (35).

By using this information together with (23) to calculate the correct value of μ at a reflection point, it is possible to reveal the same structures of the map created by numerical solutions of the equations of motion. The locations of each main resonance are approximately the same as those found by the mapping equation (34). The advantages of using the mapping equation are clearly seen here. It takes an extremely long time to compute orbits that posses low values of the magnetic moment since such orbits execute very large distances before being reflected back to the median plane. The exponentially divergent behavior of chaotic trajectories also produces numerical errors in the integrator which grow exponentially with time.

III. Global Behavior and a Q-dependence Map

All of the above results are subsumed in a so-called Fermi-like map (34), which gives us an overview of the global particle behavior. The typical global behavior of particle motion can be summarized by considering the structure of the Fermi map for $Q=4$ shown in Fig. 5. For a certain range

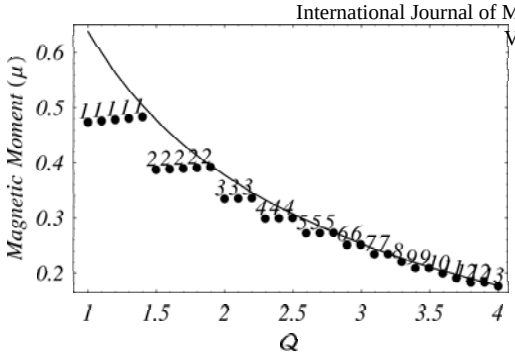

Fig. 8. $K > 4$ resonance positions. Dots indicate resonance positions at (Q, μ) that have the value of $K > 4$ while numbers indicate islands' periods or resonance numbers. The boundary of complete chaos is indicated by the line.

of μ, for example, from 0.24 to 0.3, the two resonant zones are well apart and the wondering of a particle trajectory is confined to a band of μ values, that is, by two KAM surfaces. Moving downwards the distance between two neighboring zones becomes smaller. At a certain value of μ the two resonances overlap and a macroscopic zone of instability appears in which the particle can wander from one resonance to another.

The criterion for global stochasticity can be obtained by many methods. According to the estimation by the method of overlapping resonances, the last KAM curve will be destroyed approximately at $K = 1$ and the system undergoes global stochasticity at $K > 4$. Once the system is chaotic over a significant part of phase space, it is necessary to introduce a quantitative method to describe this pseudo-random motion. Such motion in the global stochastic sea can be modeled by a diffusion process [12], [11].

Fig. 8 indicates that when $Q < 1.5$, there are no stable islands because the all islands are destroyed. However, this family of periodic solution is different from the one reported in [13].

IV. Discussion

The analysis is begun by transforming the relevant equations and definitions from the usual rectangular co-ordinate system to a hyperbolic co-ordinate system. These equations are then scaled so as to express them in a convenient form to apply multiple time perturbation theory with $\epsilon = 1/Q$ taking the place of the expansion parameter. The results give that the magnetic moment is adiabatic invariant when the particle was in high field regions. This property is confirmed by the expansion of the adiabatic invariant as suggested by the adiabatic theory. However, in general the adiabatic property of the magnetic moment breaks down when the particle crosses the low field region which is situated at the median plane $(x = y)$ for the case $Q > 1$ as in our system.

It is found that the magnetic moment oscillates violently when the solution is near or around the null point and is adiabatically constant when the solution is far away from it. Numerical calculation of the adiabatic invariant shows sudden jumps which cannot be described by the expansion of the variation in time of the magnetic moment. This phenomenon, known as non-adiabatic behavior, could be associated with the singularity in the complex plane which can be used to approximately quantify the jumps [7].

All of these results can then be subsumed in a so-called Fermi-like map (34), which gives an overview of the global particle behavior for all $Q > 1$. As μ decreases to a normalized value of what is called μ_{crit}, the corresponding normalized map becomes the standard map with $K > 4$. The behavior becomes completely chaotic and μ can diffuse down to a very small value which normally takes an infinite time to trace its trajectory. μ_{crit} moves up to the value 0.5 when Q approaches 1. This means that the global chaotic behavior occupies a larger area of the map. In other words, the particle motion is more regular when Q is large.

It is important to note that the adiabatic approximation developed here for the case $Q > 1$ is also applicable to the adiabatic case in $Q < 1$ as well, but now the confinement zone for $Q < 1$ is no longer shaped like a magnetic bottle. Furthermore, there exists a null point at the center of the confinement zone. The phase space of s_0 is qualitatively different at the center (Fig. 3). For $Q > 1$, there exists a noticable region of unsqueezing, while for $Q < 1$, all lines are joined at the center resulting in complete mixing. Most particle trajectories in this family can be concluded to behave chaotically, especially for $Q = 0$.

Acknowledgments

I would like to thank Prof.Dr. George Rowlands for fruitful discussion and invaluable guidance. This work was partially supported by the Thailand Research Fund, through the Post-Doctoral Grant (PDF/62/2540), and Walailak University under the Key University Research Unit development scheme (CX-KURUE) to Complex System Research Unit.

References

[1] P. Collas, D. Klein, and H. Schwebler, *CHAOS*, vol. 8 (2), p. 262, 1998.
[2] P. Dahlqvist and G. Russberg, *Phys. Rev. Lett.*, vol. 65 (23), p. 2837, 1990.
[3] ——, *J. Phys.*, vol. A 24, p. 4763, 1991.
[4] K. Jaroensutasinee and G. Rowlands, *J. Plasma Phys.*, vol. 63 (3), p. 255, 2000.
[5] M. G. Rusbridge, *Plasma Phys.*, vol. 13, p. 977, 1971b.
[6] ——, *Plasma Phys.*, vol. 19, p. 1087, 1977.
[7] J. Howard, *Phys. Fluids*, vol. 14, p. 2373, 1971.
[8] A. H. Nayfeh and D. T. Mook, "Nonlinear oscillations," *John Wiley & Sons*, 1979.
[9] B. V. Chirikov, *Phys. Reports*, vol. 52, p. 265, 1979.
[10] V. D. Il'in, S. N. Kuznetsov, and B. Y. Yushkov, *JETP Lett.*, vol. 55 (11), p. 645, 1992.
[11] A. J. Lichtenberg and M. A. Lieberman, *Regular and Stochastic Motion*, vol. Springer-Verlag, 1983.
[12] S. G. Tagare, *Phys. Rev. A*, vol. 34, no. 2, pp. 1587–1590, Aug 1986.
[13] K. Jaroensutasinee and G. Rowlands, *J. Phys.*, vol. A 27, p. 1163, 1994.